Time-optimal universal control of two-level systems under strong driving

C. Avinadav, R. Fischer, P. London, and D. Gershoni

Department of Physics, Technion, Israel Institute of Technology, Haifa 32000, Israel

We report on a theoretical and experimental study of time-optimal construction of arbitrary single-qubit rotations under a single strong driving field of finite amplitude. Using radiation-dressed states of nitrogen vacancy centers in diamond we realize a strongly driven two-level system, with driving frequencies four times larger than its precession frequency. We implement time-optimal universal rotations on this system, characterize their performance using quantum process tomography, and demonstrate a dual-axis multiple-pulse control sequence where the qubit is rotated on time scales faster than its precession period. Our results pave the way for applying fast qubit control and high-density pulse schemes in the fields of quantum information processing and quantum metrology.

I. INTRODUCTION

Two-level systems are the prototypical realization of a quantum bit (qubit), and as such, coherent control of their state is a key element in novel quantum devices and applications. Two important measures of qubit control techniques are the *time* it takes to complete a desired rotation, and the ability to perform *arbitrary* state rotations within a given realization. Reduced manipulation times allow for an increased number of operations to be performed within the system coherence time, a critical requisite of quantum information processing [1] and quantum sensing [2]. Similarly, the ability to perform universal single-qubit rotations [3,4] can reduce the complexity of quantum computing algorithms as opposed to utilizing only a minimal set of single-qubit gates [5,6]. Universal rotations are also useful in pulsed quantum sensing schemes [7], as they allow for systematic pulse error compensation using composite pulses [8,9] or multiple-axis decoupling techniques [10–12].

Generally, the rotation time of a qubit's state depends on the strength of the fields applied to it. Obtaining shorter manipulation times therefore requires stronger driving fields, eventually leading to the strong driving regime. In this regime the qubit is driven by an external field whose coupling energy is comparable to, or exceeds, the energy level splitting of the qubit itself. The traditional method of applying an oscillatory field at the qubit's resonance frequency results in complex dynamics under strong driving, due to the counter-rotating term of the oscillating field. This term can be neglected for weak driving according to the rotating wave approximation [13,14], but for strong fields it plays a crucial role in the system dynamics [15,16]. Therefore, different control schemes have been considered for this regime, including usage of ancillary energy levels [4], two independent orthogonal fields [17,18], or single-field anharmonic pulses.

Considering the approach of anharmonic pulse sequences it was shown, with tools of optimal control theory, that the fastest way to steer a qubit on the Bloch sphere from one state to another, using a single driving field of finite amplitude $|B(t)| \leqslant B_{\max}$, is a *bang-bang* control [19,20], i.e., rectangular pulses alternating between the extremal values of the driving field $\pm B_{\max}$. This approach was recently applied also to the Landau-Zener problem, for finding the "quantum speed limit," the minimal time required to transfer a system between any

two states [21]. However, these studies considered only the problem of steering the system state between two points on the Bloch sphere, rather than generating a prescribed rotation operator. Thus, for example, these results cannot be applied for achieving π-flips around an *arbitrary* rotation axis. The challenge of generating *any* desired unitary operator was previously studied only for weak driving [22] or under the assumption of infinitely strong driving fields [23].

In this work we present a theoretical and experimental study of time-optimal universal qubit rotations in the strong driving regime. We derive the necessary conditions that must be satisfied by a pulse sequence in order to be time optimal, and through numerical optimization design pulses for the important cases of $\pi/2$ and π rotations around arbitrary axes in the Bloch sphere's equatorial plane. Then, we experimentally apply these control sequences on radiation-dressed states of electron spins in nitrogen-vacancy (NV) centers in diamond. This approach enables us to realize a strongly driven two-level system with excellent controllability and superior coherence properties with respect to bare NV spin. Finally we use this system to apply a dual-axis multiple-pulse sequence with an unprecedented interpulse delay of two spin precession periods.

II. TIME-OPTIMAL SYNTHESIS OF UNIVERSAL ROTATIONS

We consider a general two-level system, or a manifold of a more complex system, driven by a single external field. It is described by the time-dependent Hamiltonian

$$H(t) = \tfrac{1}{2}\hbar\omega_1\sigma_z + \tfrac{1}{2}\hbar\Omega(t)\sigma_x, \qquad (1)$$

where ω_1 is the energy level splitting, or the spin precession frequency, $\Omega(t)$ is the applied driving field bounded by $|\Omega(t)| \leqslant \Omega_{\max}$, and σ_i are the Pauli matrices, where $\hat{x}$ is the direction of the applied external field. The time evolution operator $U(t)$ represents the rotation induced by the control sequence $\Omega(t)$, and evolves in time according to

$$i\hbar\dot{U}(t) = H(t)U(t), \qquad (2)$$

with $U(0) = I_{2\times2}$. In this formalism, the problem of generating a time-optimal rotation can be regarded as that of steering the operator $U(t)$, which lies in SU(2), in minimal time onto the desired rotation U_{final}. We solve this problem in a
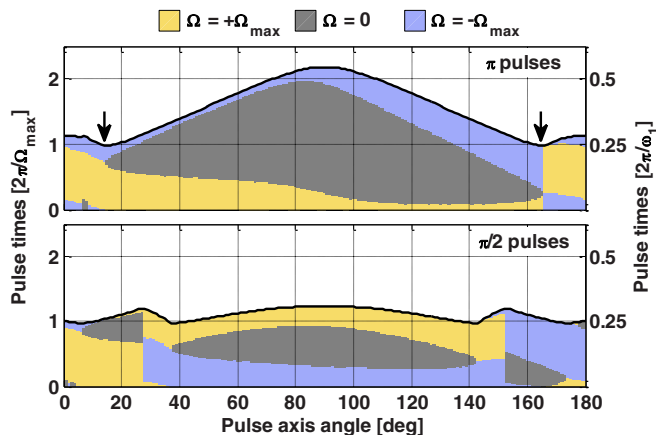
FIG. 1. (Color online) Time-optimal pulse sequences for generating $\pi/2$ and π rotations (top and bottom panels, respectively), for $\Omega_{max} = 4\omega_1$. Colors represent different types of pulses: positive/negative bangs and drift. Black arrows mark the globally optimal π rotations, corresponding to pure bang-bang controls.

two-step process of *reduction* and *selection*. First, we apply Pontryagin's minimum principle (PMP) [24,25] which gives the necessary conditions that a control $\Omega(t)$ must satisfy in order to be optimal, thus reducing substantially the number of optimal control candidates. Second, we select from these candidates the control sequences which satisfy the problem, i.e. generate the desired rotations, and choose the one which does so in minimal time. We outline these steps below and present the resulting time-optimal controls.

First, using Pontryagin's minimum principle we prove in the Appendix that time-optimal control sequences consist only of *bang periods*, in which $\Omega(t) \equiv \pm\Omega_{max}$ and the qubit rotates about an axis $\omega_1\hat{z} \pm \Omega_{max}\hat{x}$, and *drift periods*, where $\Omega(t) \equiv 0$ and the qubit simply precesses around the z axis. Remarkably, any desired single-qubit operator may be constructed in this way. This result substantially reduces the number of candidate sequences for optimal control. Finding the optimal sequence therefore amounts to selecting the correct number, ordering and length of the bang and drift periods. While this is still a challenging problem to solve analytically, it can be approached by numerical optimization on an n-dimensional space, where n is the assumed number of bang or drift periods and the optimization variables represent their durations. These durations are bounded, as the dynamics under bang or drift controls are periodic, with $T_b = 2\pi/\sqrt{\omega_1^2 + \Omega_{max}^2}$ or $T_d = 2\pi/\omega_1$, respectively. Since each pulse may either be a positive bang, a negative bang, or a drift, the optimization is repeated $3 \times 2^{n-1}$ times to explore all unique pulse sequences [26]. Using this method we verified up to $n = 12$ that three pulses or less are sufficient to construct any rotation operator, in the strong driving regime $\Omega_{max} \geqslant \omega_1$, in agreement with the ansatz made in [21].

We then set to calculate the pulse sequences that generate time-optimal $\pi/2$ and π rotations around different axes in the x-y plane (Fig. 1). In the case of π pulses we note the following: (a) for $\Omega_{max} \gg \omega_1$ the duration of the *longest* control sequence approaches π/ω_1, corresponding to half a precession cycle of the spin inserted between two δ-like $\pi/2$ rotations; (b)

the *shortest* control sequence consists of two opposite bang periods and lasts exactly $2\pi/\sqrt{\omega_1^2 + \Omega_{max}^2}$, independent of the ratio of Ω_{max} to ω_1. These two results are consistent with previous studies of infinite-amplitude fields [23] and shortest possible spin flips [19,20].

III. EXPERIMENTAL SYSTEM

We use radiation-dressed states of the electron spin of nitrogen-vacancy (NV) centers in diamond [27] to realize a strongly driven two-level system, and to implement the control sequences described above. This approach of using dressed states as an effective two-level system can be applied to many different physical systems, and it offers, among other advantages which will be explained below, a high degree of controllability of the system and extended coherence times [28]. The scheme is based on resonant microwave radiation interacting with the NV center electron spin, thereby creating a dressed two-level system whose energy level splitting is determined by the coupling energy of the dressing field. A second magnetic field, orthogonal to the resonant microwave field, is used to manipulate the state of the dressed qubit on its Bloch sphere.

A. Radiation-dressed states of NV centers

The NV center has a spin triplet ($S = 1$) ground state [Fig. 2(a)]. It can be optically pumped into the $m_s = 0$ state
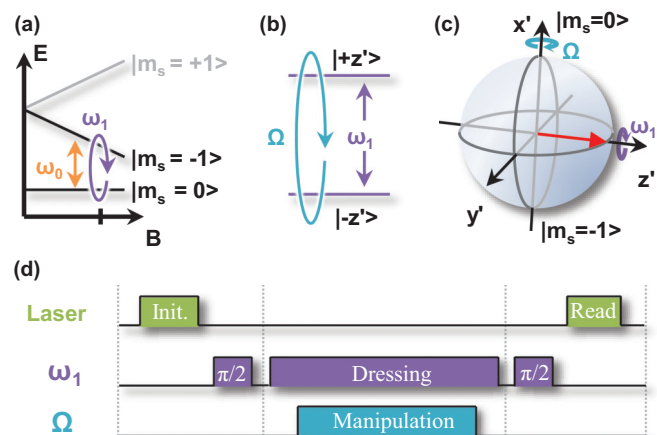

FIG. 2. (Color online) (a) Energy level structure of the NV center ground state in the presence of axial magnetic field B, which lifts the degeneracy between the $m_s = \pm 1$ states. (b) Applying continuous microwave excitation resonant with the $m_s = 0, -1$ transition creates new dressed states with an energy separation ω_1, determined by the Rabi frequency of the dressing field. (c) Bloch sphere representation of the electron spin in the $m_s = 0, -1$ subspace. The continuous driving field ω_1 defines the new z' axis of the dressed qubit basis, and the second-order driving $\Omega(t)$ acts in an orthogonal direction, enabling manipulation of the dressed states. (d) Experimental sequence: initialization of the dressed spin by optical pumping and a microwave $\frac{\pi}{2}$ pulse; manipulation of the dressed spin with the second-order field $\Omega(t)$, while the microwave field continuously dresses the spin; and readout of the dressed spin projections by a microwave $\frac{\pi}{2}$ pulse and optical readout of the bare spin population.

with a short laser pulse, and its population can be measured by spin-dependent photoluminescence [29]. A magnetic field of 540 G aligned to the NV z axis lifts the degeneracy of the $m_s = \pm 1$ states and enables selective microwave excitation of the $m_s = 0, -1$ transition at $\omega_0 = (2\pi)1.36$ GHz. This selectivity allows us to consider only the $m_s = 0, -1$ states of the NV center spin, corresponding to the $|+z\rangle$ and $|-z\rangle$ eigenstates of a pseudo-spin-$\frac{1}{2}$ system, while the $m_s = +1$ state is well out of resonance with any of the applied fields and does not participate in the system dynamics.

We write the system Hamiltonian as

$$H(t) = \tfrac{1}{2}\hbar\omega_0\sigma_z + \hbar\omega_1\cos(\omega_0 t)\sigma_x + \tfrac{1}{2}\hbar\Omega_{\max}A(t)\sigma_z, \quad (3)$$

where the first term corresponds to the unperturbed Hamiltonian of the pseudo-spin-$\frac{1}{2}$, the second term describes the resonant microwave field applied along the NV center x axis (chosen arbitrarily) that creates the dressed qubit, and the third term is the second-order magnetic field applied along the z axis that allows manipulation of the dressed qubit states. ω_0 is the splitting between the two bare spin eigenstates ($m_s = 0, -1$), ω_1 is the Rabi frequency of the dressing field, and $\Omega_{\max}$ is the maximum amplitude of the second-order field with $A(t)$ its envelope function. In the interaction picture of $H_0 = \tfrac{1}{2}\hbar\omega_0\sigma_z$ and under the rotating wave approximation (RWA) for $\omega_1 \ll \omega_0$, the Hamiltonian becomes

$$\tilde{H}(t) = \tfrac{1}{2}\hbar\omega_1\sigma_x + \tfrac{1}{2}\Omega_{\max}A(t)\sigma_z. \quad (4)$$

Upon the rotation $(x, y, z) \rightarrow (z', y', -x')$, which represents the transformation into the dressed-states basis [Figs. 2(b)–2(c)], this Hamiltonian exactly manifests the prototypical Hamiltonian of Eq. (1). It describes the dressed qubit, a two-level system with energy level splitting $\hbar\omega_1$, whose eigenstates correspond to the $|+x\rangle$ and $|-x\rangle$ states of the bare NV electron spin in the rotating frame. The dressed qubit is driven by a time-dependent transverse field $\Omega_{\max}A(t)$. Thus, by tuning the ratio between $\Omega_{\max}$ and ω_1 one can switch between the weak and strong driving regimes, and study various manipulation techniques using different envelope functions $A(t)$. Our experiments were conducted with the parameters $\omega_1 = (2\pi)1.5$ MHz and $\Omega_{\max} = (2\pi)6$ MHz, representing a driving field four times stronger than the dressed spin's precession frequency.

Experiments on the dressed qubit consist of three stages: arbitrary state initialization, pulsed manipulation, and tomographic state readout [Fig. 2(d)]. The dressed qubit is initialized to $|+z'\rangle$ by optically pumping the spins into the $|+z\rangle$ state (corresponding to $m_s = 0$) using a short laser pulse, and then rotating them to $|+x\rangle$ by a $(\frac{\pi}{2})_y$ rotation induced with a short pulse of the microwave field. Similarly, to measure the dressed qubit's z' projection we apply the same sequence in reverse, i.e., a $(\frac{\pi}{2})_y$ pulse followed by a laser pulse to readout the $m_s = 0$ population of the bare spins. By changing the duration and rotation axis of the $\frac{\pi}{2}$ pulses in either stage we may initialize the dressed spin into different states or measure different projections of it, thereby enabling arbitrary initialization and complete state tomography of the dressed qubit.

B. Advantages of using the dressed spin

Using the radiation-dressed spin in this experimental study of fundamental control in quantum systems offers several distinct advantages over the bare spin system:

(a) The dressed spin is protected from spurious magnetic noise via continuous dynamical decoupling [30–32]. In our setup, we measured a tenfold improvement in the phase-memory time T_2^* from 0.7 to 7 μs.

(b) The dressed spin accurately manifests the Hamiltonian [Eq. (1)], and specifically is insensitive to the alignment of the second-order driving field $\Omega(t)$: any x or y components of this field average to zero in the rotating frame under the RWA since $\Omega_{\max} \ll \omega_0$, resulting in pure transverse driving of the dressed spin and eliminating dynamical energy shifts that may cause unwanted coupling between its states.

(c) The dressed spin is a better representation of a true two-level system than the bare system, which may include additional energy states. This is particularly important for the application of bang-bang control sequences, which are intrinsically wideband and may therefore cause unwanted coupling to these additional energy levels [33]. With this analogy to a two-level system in mind, and for the sake of brevity, henceforth we refer to the dressed spin simply as a qubit or a spin.

C. Harmonic driving of the dressed spin beyond the RWA

Here we demonstrate the dressed spin dynamics under resonant harmonic excitation; i.e., $\Omega(t) = \Omega_{\max}\cos(\omega_1 t)$. In a frame rotating at ω_1 this field is rewritten as the sum of two terms, $\Omega(t) = \Omega_{\max}[1 + \exp(2i\omega_1 t)]/2$. The first term is fixed in the rotating frame, while the second rotates at twice the precession frequency ω_1. At the weak driving regime, $\Omega_{\max} \ll \omega_1$, the second term averages to zero—this is the rotating wave approximation—and the resulting spin dynamics are the familiar Rabi oscillations, occurring at a frequency $\Omega_{\max}$ [Fig. 3(a)] [34].

However if we attempt to shorten the spin manipulation time by increasing the field amplitude, the counter-rotating term becomes non-negligible and the dynamics differ significantly from the expected result in both the z' projection of the spin and its x'-y' components [Figs. 3(b)–3(c)]. These results show a clear signature of a strongly driven two-level system. It is important to note that while the dressed spin does rotate on time scales much shorter than its precession period in Fig. 3(c) for $\Omega_{\max}/\omega_1 = 1.5$, the first "dip" of the oscillations that occurs at $t = 0.25 \times (2\pi/\omega_1)$ does not correspond to an actual spin flip; i.e., the spin does not reach the south pole of the Bloch sphere. It is only on the third dip, at $t = 1.25 \times (2\pi/\omega_1)$, that the spin actually reaches this state, demonstrating the inefficiency of the harmonic driving method at such strong fields.

IV. DEMONSTRATION OF TIME-OPTIMAL CONTROLS AND THEIR APPLICATION

A. Characterization of time-optimal π pulses

We implemented the driving scheme described in Sec. II on an ensemble of NV centers using the dressed spin as the prototype two-level system, and measured the performance of the designed time-optimal π pulses. We first illustrate the spin
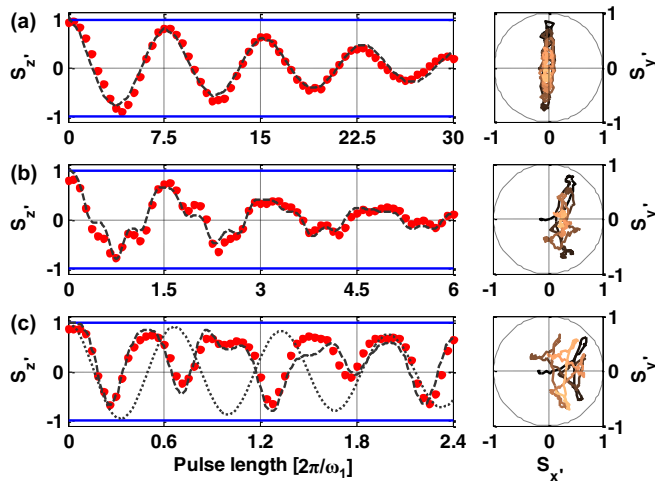
FIG. 3. (Color online) Harmonic driving of the dressed spin at increasing coupling strengths: (a) $\Omega_{max}/\omega_1 = 0.16$, (b) $\Omega_{max}/\omega_1 = 0.67$, and (c) $\Omega_{max}/\omega_1 = 1.5$. Left panels show the z' component of the spin (dots: experiment, thick dashed line: simulation, thin dotted line: expected Rabi oscillations without the counter-rotating term) and right panels show the spin trajectory in the x'-y' plane (measurements only, time flows from dark to bright colors). An exponential decaying envelope was fitted to the measurements and applied to the simulation results for comparison purposes.

dynamics under such pulses in detail. For a bang-bang control sequence bounded by $\Omega_{max} = 4\omega_1$, the qubit is rotated on time scales faster than its precession frequency ω_1 [Fig. 4(a)]. The measured state trajectory on the Bloch sphere under this sequence [Fig. 4(b)] fits the predicted behavior well: the first bang rotates the qubit from the north pole $|+z'\rangle$ to the equator, failing to pass through the desired south pole $|-z'\rangle$ due to the nonvanishing free precession ω_1. The second bang, of opposite
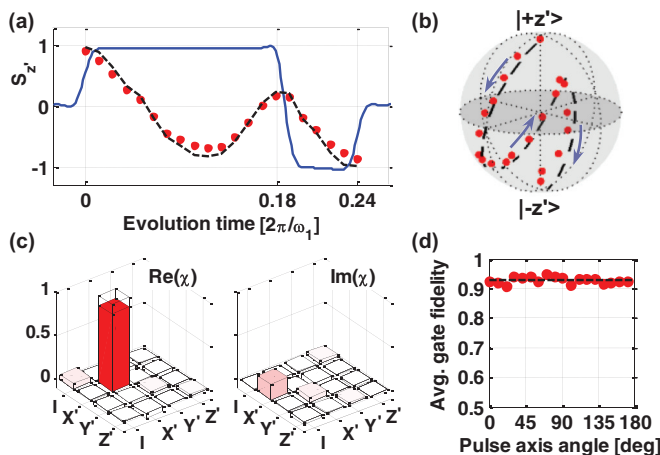

FIG. 4. (Color online) (a) and (b): Measurement of the spin z' component and its full state trajectory, respectively, under a bang-bang sequence (red dots: experiment, black dashed line: simulation, blue solid line: pulse sequence in units of Ω_{max}; arrows denote the flow of time). (c) Real and imaginary parts of the measured process matrix for $\pi_{x'}$ pulse (empty bars show the ideal matrix). (d) Measured gate fidelities of π pulses around different axes in the x'-y' plane. Average fidelity obtained was 0.93 ± 0.01.

sign, compensates for this effect and completes the π pulse by rotating the qubit exactly to $|-z'\rangle$.

A complete characterization of universal spin-flip sequences was carried out using quantum process tomography [35]. Figure 4(c) shows the measured process matrix for a π pulse around the x axis, with an average gate fidelity [36] of 0.92. π flips around different axes in the x-y plane were also characterized [Fig. 4(d)]. We measure an average gate fidelity of 0.93 ± 0.01. The fidelity is limited by our technical ability to deliver ideal bang-bang pulses, and does not represent a fundamental limit of our spin control technique. These results demonstrate our ability to perform universal qubit rotations at time scales much shorter than the qubit's precession period. Achieving similar controllability using traditional harmonic driving requires at least an order of magnitude *slower* dynamics than the precession period in order to satisfy the RWA and to maintain high fidelity.

B. Application of time-optimal control in quantum protocols

In addition to quantum information processing, fast arbitrary-axis rotations also play a key role in ac magnetometry sequences, aimed at detecting classical sources emitting ac magnetic fields [2,37] or the fluctuating fields of nearby spins [38,39]. One such sensing scheme is based on repeatedly applying π pulses to the sensing spin at regular intervals [38,40], similar to pulsed dynamical decoupling sequences [41,42]. This acts as a lock-in measurement, significantly increasing the sensitivity of the spin to ac magnetic fields at frequencies matching the interpulse delay. Keeping this delay fixed and increasing the number of π pulses improves the sensitivity and narrows the frequency response function. However two deteriorating mechanisms compete with this improvement: (a) the total sequence time increases linearly with the number of pulses while the coherence time improves only sublinearly [11,43], exposing the spin to decoherence; (b) errors in the π pulses accumulate and decrease the overall signal fidelity.

The effect of pulse error accumulation can be mitigated by implementing multiple-axis control over the spin and by symmetrizing the pulse sequence [10–12] [Fig. 5(a)]. Figure 5(b) shows the performance of dual-axis XY4-N and XY8-N sequences, implemented using the time-optimal π pulses which were characterized above, compared to a single-axis sequence implemented with the same pulses. A substantial suppression in the pulse error accumulation is indicated by the slower decay coherence as the number of π pulses is increased. Furthermore, the interpulse delay τ in these sequences was set to only two precession periods of the spin, representing a regime of high pulse density which is unreachable with weak harmonic driving techniques.

V. SUMMARY AND OUTLOOK

In this work we studied, both theoretically and experimentally, the time-optimal construction of arbitrary single-qubit rotations under a single strong driving field of finite amplitude. We showed that arbitrary time-optimal rotations of two-level systems are constructed as a series of bang pulses and drift periods, and that under a strong driving field a combination of
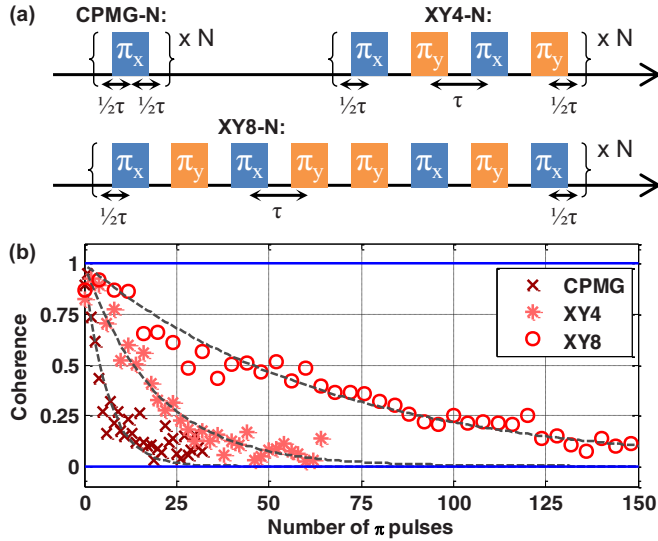
FIG. 5. (Color online) Demonstration of ac magnetometry sequences using two-axis control in the strong driving regime. (a) CPMG-N: a fixed-axis π_x pulse is applied N times at regular intervals; XY4-N and XY8-N: the sequences π_x-π_y-π_x-π_y and π_x-π_y-π_x-π_y-π_y-π_x-π_y-π_x, respectively, are applied N times. At the beginning and end of each sequence a $(\pi/2)_x$ pulse is applied. (b) Measured coherence as a function of the total number of π pulses, under different decoupling sequences (symbols: experiment, dash lines: exponential decay fits). In all cases the interpulse delay was two precession periods ($4\pi/\omega_1$).

three such pulses can be used to obtain general rotations on the Bloch sphere. This result is general to any driven two-level system and may be applied to different physical realizations such as quantum dots, donors in semiconductors, trapped ions, and superconducting flux qubits.

Importantly, our result allows for designing arbitrary *rotations*, or single-qubit gates, rather than just steering the state of the system from one point on the Bloch sphere to another, which is a crucial requirement for implementations of quantum information processing or quantum metrology. As an example, being able to apply π rotations around different axes on the Bloch sphere is a requisite for universal dynamical decoupling sequences [11], as we demonstrated in our study. This new regime of high-density pulse sequences, where pulses are shorter than the qubit's precession period and their spacing also approaches this time scale, can enable, for instance, quantum sensing of high-frequency fields or efficient suppression of wideband decoherence processes.

Finally, in our study we used the dressed spin as a prototypical two-level system with several key advantages: it benefits from longer coherence times compared to the bare spin of the NV center, it is a more accurate and robust realization of a true two-level system, and it offers better controllability over the system parameters and the driving field. Most importantly, it allows a straightforward and technically easy approach to a strongly driven quantum system, thus enabling fundamental research of different manipulation techniques in this regime.

APPENDIX: NECESSARY CONDITIONS ON TIME-OPTIMAL UNIVERSAL CONTROLS

We provide here a complete proof that time-optimal control sequences, for the problem presented in the main text, consist only of bang pulses ($\Omega = \pm\Omega_{\max}$) and drift periods ($\Omega = 0$). A similar proof can be found in Ref. [19] of the main text. We begin by parametrizing the time-evolution operator $U(t)$ using three Euler angles,

$$U(\psi,\theta,\phi) = \exp\left(\tfrac{1}{2}i\psi\sigma_z\right)\exp\left(\tfrac{1}{2}i\theta\sigma_y\right)\exp\left(\tfrac{1}{2}i\phi\sigma_z\right), \quad \text{(A1)}$$

and define the state vector $\mathbf{x}(t) = (\psi(t),\theta(t),\phi(t))$. From Eqs. (1) and (2) we find the equations of motion for this vector,

$$\begin{aligned} \dot{\psi} &= \omega_1 - \Omega\cos\psi\cot\theta, \\ \dot{\theta} &= -\Omega\sin\psi, \\ \dot{\phi} &= \Omega\cos\psi\csc\theta. \end{aligned} \quad \text{(A2)}$$

We now apply Pontryagin's minimum principle (PMP) [24,25] which gives the necessary conditions that a control $\Omega(t)$ must satisfy in order to be optimal, thus reducing substantially the number of optimal control candidates. The principle states the following: given a state vector $\mathbf{x}$ which satisfies a dynamical system $\dot{\mathbf{x}}(t) = f(\mathbf{x}(t),\Omega(t);t)$, where $\Omega(t)$ is a bounded control, we construct the Pontryagin Hamiltonian

$$H_P(\mathbf{x}(t),\mathbf{p}(t),p_0,\Omega(t);t) = \mathbf{p}\cdot\dot{\mathbf{x}} + p_0. \quad \text{(A3)}$$

Here $\mathbf{p}(t)$ is the costate vector, satisfying the adjoint equation $\dot{\mathbf{p}} = -\partial H_P/\partial\mathbf{x}$, and p_0 is a nonnegative constant chosen such that $\mathbf{p}(t)$ and p_0 do not vanish together at all times (*nontriviality condition*). According to the PMP, a necessary condition for a control $\Omega(t)$ to be optimal is to maximize the Pontryagin Hamiltonian $H_P(t)$ at all times. Additionally H_P must vanish at the final time (*transversality condition*). For time-optimal problems in which H_P has no explicit time dependence, it can be shown to be constant and equal to zero at all times under optimal control [44].

Using Eqs. (A2) we construct the Pontryagin Hamiltonian for our problem,

$$\begin{aligned} H_P(\mathbf{x},\mathbf{p},p_0,\Omega) = &-\Omega(p_1\cos\psi\cot\theta + p_2\sin\psi \\ &- p_3\cos\psi\csc\theta) + p_1\omega_1 + p_0, \end{aligned} \quad \text{(A4)}$$

with the costate vector $\mathbf{p}(t) = (p_1(t),p_2(t),p_3(t))$. We find that H_P is linear in Ω, and we define its coefficient $\Phi(\mathbf{x},\mathbf{p};t) = \partial H_P/\partial\Omega$. At times where $\Phi(t)$ is nonzero the Pontryagin Hamiltonian is indeed a linear function of Ω, and it obtains its maximum at the edges of the allowed control range,

$$\Omega(t) = \begin{cases} +\Omega_{\max} & \Phi(t) > 0, \\ -\Omega_{\max} & \Phi(t) < 0. \end{cases} \quad \text{(A5)}$$

However when vanishes $\Phi(t)$ identically—on a so-called *singular arc*—H_P becomes independent of Ω and the maximization principle cannot be used to constrain it. Nevertheless we now show, based on the nontriviality and transversality

conditions, that on a time interval where $\Phi(t)$ is identically zero, the control $\Omega(t)$ must be zero as well. To this end, we write explicitly Φ as

$$\Phi(\mathbf{x},\mathbf{p};t) = \frac{\partial H_P}{\partial \Omega}$$
$$= p_1 \cos\psi \cot\theta + p_2 \sin\psi - p_3 \cos\psi \csc\theta. \quad (A6)$$

We also write the equations for the costate vector $\mathbf{p}(t) = (p_1(t), p_2(t), p_3(t))$ as derived from $\dot{\mathbf{p}} = -\partial H/\partial \mathbf{x}$,

$$\dot{p}_1 = \Omega(-p_1 \sin\psi \cot\theta + p_2 \cos\psi + p_3 \sin\psi \csc\theta), \quad (A7)$$

$$\dot{p}_2 = \Omega(-p_1 \cos\psi \csc^2\theta + p_2 \sin\psi$$
$$+ p_3 \cos\psi \csc\theta \cot\theta), \quad (A8)$$

$$\dot{p}_3 = 0. \quad (A9)$$

We now set $\Phi(t) = 0$ in Eq. (A6), and find that p_1 can be written as

$$p_1 = -p_2 \tan\psi \tan\theta + p_3 \sec\theta. \quad (A10)$$

Also on a singular arc the Hamiltonian (A4) has the form $H_P = p_1 \omega_1 + p_0$, and since it is an integral of the problem, p_1 must be constant on singular arcs. Substituting Eq. (A10)

into Eq. (A7) and setting $\dot{p}_1 = 0$ we obtain

$$\Omega p_2 \sec\psi = 0, \quad (A11)$$

so that either $\Omega = 0$ as required, or $p_2 = 0$. Assuming the latter, we then must also have $\dot{p}_2 = 0$ on the singular arc, and we find from substituting Eq. (A10) into Eq. (A8) and setting $p_2 = \dot{p}_2 = 0$,

$$-\Omega p_3 \cos\psi \sec\theta = 0. \quad (A12)$$

Again this means that either $\Omega = 0$ as required, or that either $\cos\psi$ or p_3 vanish identically on the singular arc. We contradict the latter two possibilities:

(1) If $\cos\psi = 0$ on some time interval then ψ must be constant on that interval. This contradicts Eq. (A2) which, for $\cos\psi = 0$, has the form $\dot{\psi} = \omega_1 \neq 0$.

(2) If $p_3 = 0$ then by Eq. (A10) we have $p_1 = 0$, since we also assumed $p_2 = 0$. This means that the costate vector $\mathbf{p}$ vanishes entirely, and the Hamiltonian (A4) is simply $H_P = p_0$. However based on the transversality condition, H_P must vanish on an optimal control, so $p_0 = 0$, and we find that $\mathbf{p} = 0$ and $p_0 = 0$ in contradiction to the nontriviality condition.

This completes the proof that $\Omega(t) = 0$ on singular arcs, i.e., for $\Phi(t) = 0$.

---

[1] D. P. DiVincenzo, Fortschr. Phys. **48**, 771 (2000).

[2] G. de Lange, D. Riste, V. V. Dobrovitski, and R. Hanson, Phys. Rev. Lett. **106**, 080802 (2011).

[3] S. Foletti, H. Bluhm, D. Mahalu, V. Umansky, and A. Yacoby, Nat. Phys. **5**, 903 (2009).

[4] Y. Kodriano, I. Schwartz, E. Poem, Y. Benny, R. Presman, T. A. Truong, P. M. Petroff, and D. Gershoni, Phys. Rev. B **85**, 241304(R) (2012).

[5] A. Galindo and M. Martín-Delgado, Rev. Mod. Phys. **74**, 347 (2002).

[6] C. M. Dawson and M. A. Nielsen, Quantum Inf. Comput. **6**, 81 (2006).

[7] N. Zhao, J. Honert, B. Schmid, M. Klas, J. Isoya, M. Markham, D. Twitchen, F. Jelezko, R.-B. Liu, H. Fedder *et al.*, Nat. Nanotechnol. **7**, 657 (2012).

[8] M. H. Levitt and R. Freeman, J. Magn. Reson. (1969) **33**, 473 (1979).

[9] L. Vandersypen and I. Chuang, Rev. Mod. Phys. **76**, 1037 (2005).

[10] T. Gullion, D. B. Baker, and M. S. Conradi, J. Magn. Reson. (1969) **89**, 479 (1990).

[11] G. de Lange, Z. H. Wang, D. Riste, V. V. Dobrovitski, and R. Hanson, Science **330**, 60 (2010).

[12] Z.-H. Wang, G. de Lange, D. Ristè, R. Hanson, and V. V. Dobrovitski, Phys. Rev. B **85**, 155204 (2012).

[13] E. Jaynes and F. Cummings, Proc. IEEE **51**, 89 (1963).

[14] M. Frasca, Ann. Phys. **306**, 193 (2003).

[15] G. D. Fuchs, V. V. Dobrovitski, D. M. Toyli, F. J. Heremans, and D. D. Awschalom, Science **326**, 1520 (2009).

[16] I. Chiorescu, P. Bertet, K. Semba, Y. Nakamura, C. J. P. M. Harmans, and J. E. Mooij, Nature (London) **431**, 159 (2004).

[17] J. H. Shim, S.-J. Lee, K.-K. Yu, S.-M. Hwang, and K. Kim, J. Magn. Reson. **239**, 87 (2014).

[18] P. London, P. Balasubramanian, B. Naydenov, L. P. McGuinness, and F. Jelezko, arXiv:1404.6282.

[19] U. Boscain and Y. Chitour, SIAM J. Control Optim. **44**, 111 (2005).

[20] U. Boscain and P. Mason, J. Math. Phys. **47**, 062101 (2006).

[21] G. C. Hegerfeldt, Phys. Rev. Lett. **111**, 260501 (2013).

[22] A. Garon, S. J. Glaser, and D. Sugny, Phys. Rev. A **88**, 043422 (2013).

[23] N. Khaneja, R. Brockett, and S. Glaser, Phys. Rev. A **63**, 032308 (2001).

[24] L. Pontryagin, *L. S. Pontryagin: Mathematical Theory of Optimal Processes*, Classics of Soviet Mathematics (CRC Press, 1987).

[25] I. M. Ross, *A Primer on Pontryagin's Principle in Optimal Control* (Collegiate Publishers, 2009).

[26] An *n*-pulse sequence that contains consecutive pulses of the same type can be considered as an $(n-1)$-pulse sequence, and need not be calculated again. Thus in constructing unique sequences we have 3 options for the initial pulse type, but only 2 options for the remaining $n-1$ pulses.

[27] F. Jelezko and J. Wrachtrup, Phys. Status Solidi (a) **203**, 3207 (2006).

[28] N. Timoney, I. Baumgart, M. Johanning, A. F. Varón, M. B. Plenio, A. Retzker, and C. Wunderlich, Nature (London) **476**, 185 (2011).

[29] N. Manson, J. Harrison, and M. Sellars, Phys. Rev. B **74**, 104303 (2006).

[30] P. Chen, Phys. Rev. A **73**, 022343 (2006).

[31] J.-M. Cai, B. Naydenov, R. Pfeiffer, L. P. McGuinness, K. D. Jahnke, F. Jelezko, M. B. Plenio, and A. Retzker, New J. Phys. **14**, 113023 (2012).

[32] X. Xu, Z. Wang, C. Duan, P. Huang, P. Wang, Y. Wang, N. Xu, X. Kong, F. Shi, X. Rong *et al.*, Phys. Rev. Lett. **109**, 070502 (2012).

[33] Z.-H. Wang and V. V. Dobrovitski, Phys. Rev. B **84**, 045303 (2011).

[34] M. Loretz, T. Rosskopf, and C. L. Degen, Phys. Rev. Lett. **110**, 017602 (2013).

[35] M. A. Nielsen and I. L. Chuang, *Quantum Computation and Quantum Information*, Cambridge Series on Information and the Natural Sciences (Cambridge University Press, 2000).

[36] The average gate fidelity is given by $F_g = (d \cdot F_\chi + 1)/(d + 1)$, where $d = 2$ is the system dimension and $F_\chi = \mathrm{Tr}[\chi_{\mathrm{meas}} \chi_{\mathrm{ideal}}]$ is the process matrix fidelity; see M. A. Nielsen, Phys. Lett. A **303**, 249 (2002).

[37] A. Laraoui, J. S. Hodges, and C. A. Meriles, Appl. Phys. Lett. **97**, 143104 (2010).

[38] T. Staudacher, F. Shi, S. Pezzagna, J. Meijer, J. Du, C. A. Meriles, F. Reinhard, and J. Wrachtrup, Science **339**, 561 (2013).

[39] F. Shi, X. Kong, P. Wang, F. Kong, N. Zhao, R.-B. Liu, and J. Du, Nat. Phys. **10**, 21 (2013).

[40] J. M. Taylor, P. Cappellaro, L. Childress, L. Jiang, D. Budker, P. R. Hemmer, A. Yacoby, R. Walsworth, and M. D. Lukin, Nat. Phys. **4**, 810 (2008).

[41] L. Viola, E. Knill, and S. Lloyd, Phys. Rev. Lett. **82**, 2417 (1999).

[42] G. S. Uhrig, Phys. Rev. Lett. **98**, 100504 (2007).

[43] N. Bar-Gill, L. Pham, C. Belthangady, D. Le Sage, P. Cappellaro, J. Maze, M. Lukin, A. Yacoby, and R. Walsworth, Nat. Commun. **3**, 858 (2012).

[44] H. Schattler and U. Ledzewicz, *Geometric Optimal Control: Theory, Methods, and Examples*, Interdisciplinary Applied Mathematics (Springer, 2012).